Journal of Power Sources 221 (2013) 345–355

Contents lists available at SciVerse ScienceDirect

Journal of Power Sources

journal homepage: www.elsevier.com/locate/jpowsour

Corrosion and thermal stability of multi-walled carbon nanotube–graphite–acrylonitrile–butadiene–styrene composite bipolar plates for polymer electrolyte membrane fuel cells

Mara Cristina Lopes de Oliveira [a], Gerhard Ett [a], Renato Altobelli Antunes [b,*]

[a] Electrocell Ind. Com. Equip. Elet. LTDA, Technology, Entrepreneurship and Innovation Center (CIETEC), 05508-000 São Paulo, SP, Brazil
[b] Engineering, Modeling and Applied Social Sciences Center (CECS), Federal University of ABC (UFABC), R. Santa Adélia 166, 09210-170 Santo André, SP, Brazil

HIGHLIGHTS

- Development of ABS–graphite–MWNT composite bipolar plates.
- EIS successfully applies for understanding the corrosion mechanism of the composites.
- MWNT concentration strongly affects the corrosion behavior of the ABS–graphite composites.
- The best balance of properties was for the ABS-graphite composite with addition of 2 wt.% MWNT.

ARTICLE INFO

Article history:
Received 26 June 2012
Received in revised form
19 August 2012
Accepted 20 August 2012
Available online 27 August 2012

Keywords:
Composite bipolar plates
PEM fuel cells
Multi-walled carbon nanotubes
Acrylonitrile–butadiene–styrene
Corrosion
TGA

ABSTRACT

Composite bipolar plates based on the proper mixing of multi-walled carbon nanotubes (MWNTs), synthetic graphite particles and acrylonitrile–butadiene–styrene (ABS) powder have been produced by hot compression molding. The corrosion properties of the molded plates were assessed through electrochemical impedance spectroscopy (EIS) and potentiodynamic polarization curves. Through-plane and in-plane electrical conductivities were determined. The relevance of electrochemical oxidation to the electrical conductivity of the composites was assessed by cyclic voltammetry. Thermal stability of the composites was examined by thermogravimetric analysis (TGA). The morphology of fractured surfaces of the plates was observed by scanning electron microscopy. The incorporation of MWNTs increased the in-plane and through-plane electrical conductivity of the ABS–graphite composites. There was, though, a corresponding reduction of the corrosion resistance. The thermal behavior was little affected by the addition of MWNTs.

1. Introduction

The development of composite bipolar plates for PEM fuel cells is a fertile research area for materials scientists [1]. In spite of the expressive accumulation of knowledge on the complex structure–property relationship of these components, several aspects are yet unexplored [2]. Corrosion resistance is an example. While metallic materials concentrate most part of the scientific investigations concerning the corrosion behavior of bipolar plates [3–6], this aspect is often disregarded for polymer–graphite composites. Such incipient research activity emerges because of the notorious chemical stability of carbon-based materials in the typical acid and humid environment of PEM fuel cells when compared to metallic alloys [7,8]. Nevertheless, it has been shown that composite bipolar plates do interact with the PEM fuel cell environment and are not immune to chemical degradation during operation. Kakati et al. [9] investigated the corrosion resistance of a composite bipolar plate prepared from a mixture of phenolic resin, graphite, carbon black and carbon fibers. They reported that the corrosion current density increased with the addition of the conductive carbon black and carbon fiber fillers. Carbon black is susceptible to electrochemical oxidation in the PEM fuel cell environment [10–12]. This chemical instability arises from the presence of numerous dangling bonds and defects in carbon blacks which are easily oxidized, leading to a high corrosion rate [13,14]. Recently, Antunes et al. [15] evidenced the deleterious effect that the incorporation of carbon black has on the corrosion stability of poly(vinylidene fluoride)–graphite composite

* Corresponding author. Tel./fax: +55 11 4996 8241.
E-mail address: renato.antunes@ufabc.edu.br (R.A. Antunes).

0378-7753/$ – see front matter © 2012 Elsevier B.V. All rights reserved.
http://dx.doi.org/10.1016/j.jpowsour.2012.08.052

in a typical PEM fuel cell environment. The growing quest for increasing electrical conductivity of polymer–graphite composites by incorporating minor carbon-based conductive fillers such as carbon black, carbon nanotubes and carbon fibers adds new issues to this scenario. As the electrical conductivity increases the corrosion resistance is expected to lessen. The correct balance between these two properties is a central point to guarantee the long-term stability of the composite bipolar plate. In this regard, the composite formulation must be carefully designed to give the best compromise between electrical conductivity and chemical stability.

Carbon nanotubes have been successfully incorporated as minor conductive fillers into polymer–graphite composites in order to enhance their electrical response for bipolar plate purposes [16–18]. Unlike carbon blacks, carbon nanotubes are resistant to electrochemical oxidation in H_2SO_4 solutions [19]. This result was perceived by several authors either at room temperature or at typical PEM fuel cell operating temperatures [20,21]. Shao et al. [22] explained this behavior by the difficult access of oxygen atoms to the closed rolled up coaxial graphene sheets of carbon nanotubes. Hung et al. [23] used electrochemical quartz crystal microbalance to assess the mass change induced by corrosion of carbon blacks and MWNTs in deaerated H_2SO_4 solution at room temperature. They showed that the highly ordered graphitic structure of MWNTs provided better corrosion resistance than the more amorphous conventional carbon black particles. It is worth mentioning that the vast majority of the studies regarding the electrochemical response of carbon nanotubes in PEM fuel cells simulating environments are based on its application as carbon catalyst supports [24,25]. However, if one thinks of the effect that these materials would have on the corrosion properties of composite bipolar plates, little knowledge is available. Moreover, it is well-established that metallic bipolar plates submitted to electrochemical polarization present a reduction of electrical conductivity [26,27]. Nevertheless, this effect has not been investigated for polymer–graphite composite bipolar plates either with CNT addition or not. Fukutsuka et al. [28] gave an interesting contribution on this subject. They determined the interfacial contact resistance of a carbon-coated austenitic stainless steel bipolar plate before and after polarization measurements. The results showed that the interfacial contact resistance of the carbon-coated bipolar plate was little affected by the polarization test whereas the bare substrate presented a significant loss of conductivity after polarization. Thus, the conductivity of the carbon surface was not impaired by the potentiodynamic polarization test.

Thermal stability is of prime interest for polymer–graphite composite bipolar plates. Polymeric matrices should withstand long-term operating conditions at temperatures typically ranging from 60 °C to 80 °C [29]. The development of high temperature PEM fuel cells may even increase the optimal service temperature of these devices, demanding further enhancements for the thermal performance of the polymers employed in the manufacturing of composite bipolar plates [30]. Both thermoplastic [31] and thermosetting resins [32] have been considered for the manufacturing of these devices. When a thermoplastic polymer is used, the composite must be cooled before being removed from the mold. Alternatively, when a thermosetting binder is used, the cooling step is not necessary and shorter processing times can be achieved [33]. This gives an irrefutable advantage of thermosetting resins toward the cost target of the Department of Energy of the US (DOE) [34]. However, recent developments have been conducted on manufacturing methods, yielding the production of high performance thermoplastic-based plates at short processing times [35]. Recyclability is considered an advantage of thermoplastics over thermosets [36].

Acrylonitrile–butadiene–styrene (ABS) copolymer provide high thermal stability with good mechanical properties, chemical resistance and processability at a relatively low cost if compared with other commercially available high performance thermoplastic resins such as polyphenylene sulfide (PPS) or polyvinylidene fluoride (PVDF) [37,38]. Notwithstanding, ABS-based composite bipolar plates have been hardly considered for this application [39]. This work gives an unprecedented contribution on the evaluation of this material for bipolar plate purposes, regarding specially its corrosion stability and thermal degradation resistance.

In this work we prepared MWNT–ABS–graphite composites using compression molding. The effect of the conductive MWNTs on the corrosion behavior of the composites was assessed using electrochemical impedance spectroscopy and potentiodynamic polarization curves. The in-plane and through-plane electrical conductivities of the molded plates were also determined. Scanning electron microscopy (SEM) analysis was used to observe the morphology of the composites. The corrosion mechanisms are discussed in connection with the morphological aspects revealed by the SEM micrographs. Furthermore, the influence of MWNTs on the thermal stability of the composites was investigated by thermogravimetric analysis (TGA).

2. Experimental

2.1. Materials and composite preparation

A commercial ABS resin in powder form was supplied by Basf. Synthetic graphite (fuel cell grade) particles with purity ≥95.0%, surface area of 1.5 $m^2\ g^{-1}$ and typical size of 40 μm were supplied by Asbury Carbons. The multi-walled carbon nanotubes were purchased from Federal University of Minas Gerais (UFMG, Brazil), presenting a surface area of 300 $m^2\ g^{-1}$ and purity ≥90.0%.

All components of the composite bipolar plates were in powder form. Five different compositions were prepared as shown in Table 1. Initially, the components were mixed in a Turbula T10B powder blender for 30 min. The MWNTs did not receive any surface treatment prior to the preparation of the composite. Then, the mixture was compression molded in a hydraulic press at 250 °C and a pressure of 400 kg cm^{-2} for 10 min, forming discs with 30 mm diameter and 3 mm thickness. After water cooling, the molded disc was removed from the mold and characterized. These samples were employed for the through-plane electrical conductivity determination and for the electrochemical tests. The samples for the in-plane electrical conductivity determination were molded according to the same parameters, but with different dimensions (130 × 12.7 × 3 mm).

2.2. Characterization

The in-plane electrical conductivity was measured by means of the four point probe method, according to ASTM D4496. A programmable current source was applied through the outer two probes and the voltage drop across the two inner probes was measured with a precision voltmeter. The electrical conductivity (σ) was calculated according to equation (1), where i is the constant

Table 1
Compositions used in the preparation of the composite bipolar plates.

Specimen	Mass (%)		
	ABS	Synthetic graphite	MWNT
S0	15	85	0
S1	15	84	1
S2	15	83	2
S3	15	82	3
S4	15	81	4
S5	15	80	5

current supplied through the sample, V is the voltage drop between two points separated by a distance d and A is the cross-sectional area of the sample:

$$\sigma = \frac{i \cdot d}{V \cdot A} \quad (1)$$

The through-plane electrical conductivity of the composites was evaluated according to the methodology described by Du and Jana [40]. The samples were placed between two pieces of conductive carbon paper (Toray). Two gold-plated copper electrodes were used to connect a power supply and the measurement devices. The measurement was performed using a hydraulic press. An increasing pressure was applied up to the typical clamping pressure of the composite bipolar plate in a PEM fuel cell (140 N cm^{-2}). A constant current of 10 A was applied by the power supply. The resulting voltage drop across the sample was registered using a digital multimeter. The resistance (R) was calculated using Ohm's law and the through-plane conductivity was determined using equation (1) with the proper sample dimensions. Six different samples were used for both the in-plane and through-plane measurements. The results reported in this work are referred to the average value of the six samples. Prior to the measurements, the samples were abraded up to #600 SiC paper to remove any polymer skin. The same surface finishing was applied to the samples prepared for the electrochemical tests.

The oxidation resistance of the composites was evaluated using cyclic voltammetry. The measurements were conducted in a three-electrode cell setup with the composite sample as the working electrode, a platinum wire as counter electrode and a saturated calomel electrode (SCE) as the reference. All the potentials mentioned in this text are given referred to the SCE. The electrolyte was comprised of 0.5 M H_2SO_4 + 2 ppm HF aqueous solution maintained at 70 °C. The scan rate was 50 mV s^{-1} and the potential range was from 0 V to +1.2 V.

Corrosion resistance was by potentiodynamic measurements and electrochemical impedance spectroscopy (EIS). A conventional three-electrode cell was used, with a platinum wire as counter electrode and a saturated calomel electrode (SCE) as the reference. The electrolyte was comprised of 0.5 M H_2SO_4 + 2 ppm HF aqueous solution maintained at 70 °C. Open circuit potential (OCP) was measured for 1 h. This duration insures free potential steady state required for EIS and potentiodynamic measurements. Impedance data were collected under OCP over a frequency range from 100 kHz to 10 mHz at 10 points per decade; a sine wave with ±10 mV amplitude was applied. The evolution of the electrochemical behavior was accompanied during 5 days of immersion. The experimental data were fitted with equivalent circuits (ECs) to give a more quantitative analysis of the EIS response. Potentiodynamic curves were acquired at a scan rate of 1.0 mV s^{-1}. All the measurements were performed with an Autolab PGSTAT 100 potentiostat/galvanostat equipped with an FRA (Frequency Response Analyser) module.

The fracture surface morphology of the composites was observed using a scanning electron microscope Leica/LEO 440i. Thermogravimetric analysis was carried out using a Shimadzu TA-50 instrument under nitrogen atmosphere with a flow rate of 50 mL min^{-1} at a heating rate of 10 °C min^{-1} ranging from the room temperature up to 1000 °C. Pure ABS was also tested for comparison purposes.

3. Results and discussion

3.1. Electrical conductivity

The effect of MWNT addition on the through-plane electrical conductivity of the composite bipolar plates is shown in Fig. 1. The measurements were made with specimens that were not immersed and with specimens that were immersed for 5 days in 0.5 M H_2SO_4 + 2 ppm HF solution at 70 °C and submitted to cyclic voltammetry. The through-plane electrical conductivity is considered to be more important than the in-plane electrical conductivity for composite bipolar plates, since the electrons must pass through the thickness of the plate [41]. As shown in Fig. 1, there is a clear trend of increasing the conductivity after incorporation of the MWNTs. The through-plane conductivities of the S1 and S2 composites are almost 300% higher than that of the S0 specimen. By increasing the concentration of MWNTs in the composite, the conductivity was little affected. It was observed that the S1 composite reached the highest conductivity mean value and the S2 composites reached the highest absolute value. It is clear that the conductivities are very similar for these composites. There is a tendency of reducing these values for higher MWNT concentrations. This effect, though only marginally detected in this work, was reported by several authors [42–44]. It is often agreed that the clustering of carbon nanotubes at high loadings reduces the electrical conductivity of polymer–MWNT composites due to the difficult dispersion of the nanofillers within the polymer matrix [45,46]. Notwithstanding, the conductivity remained far higher than that of the MWNT-free composite up to an MWNT concentration of 5 wt.%. These results evidence the beneficial effect of incorporating the nanofillers into the ABS–graphite composites. The immersion period did not present a detectable effect on the through-plane conductivity of the composites as shown in Fig. 1. The values obtained after immersion are very similar to those measured before immersion. This suggests that the samples were not significantly oxidized during the test, maintaining its electrical performance. This subject was further investigated through cyclic voltammetry measurements.

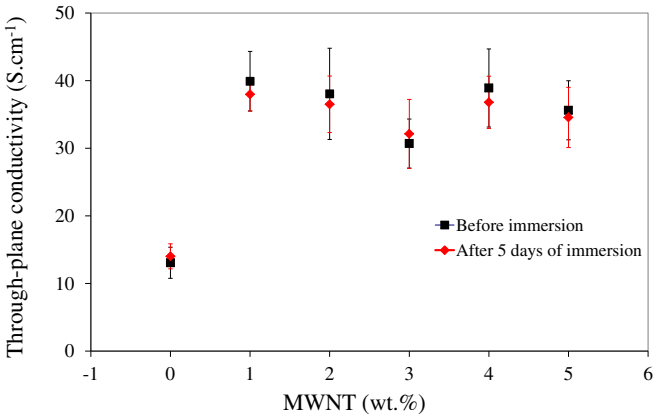

Fig. 1. Through-plane electrical conductivity of the composites plotted as a function of the MWNT content. The measurements were made with specimens before immersion and after 5 days in 0.5 M H_2SO_4 + 2 ppm HF solution at 70 °C and submitted to cyclic voltammetry.

Cyclic voltammetry was used to study the oxidation behavior of the composites in 0.5 M H_2SO_4 + 2 ppm HF solution at 70 °C after different periods of immersion. The results are shown in Fig. 2. The stability of the samples is clearly visible. The most striking feature of the voltammograms is an oxidation peak during the cathodic scan at approximately +0.2 V for all the composites. The intensity of this peak is higher for the MWNT–containing composites. It is noted that the peak is reduced with time, suggesting that the oxidation of the composites was not accelerated during immersion in the electrolyte. This result can be used to support the observation that the through-plane electrical conductivity of the composites was little affected after immersion as shown in Fig. 1.

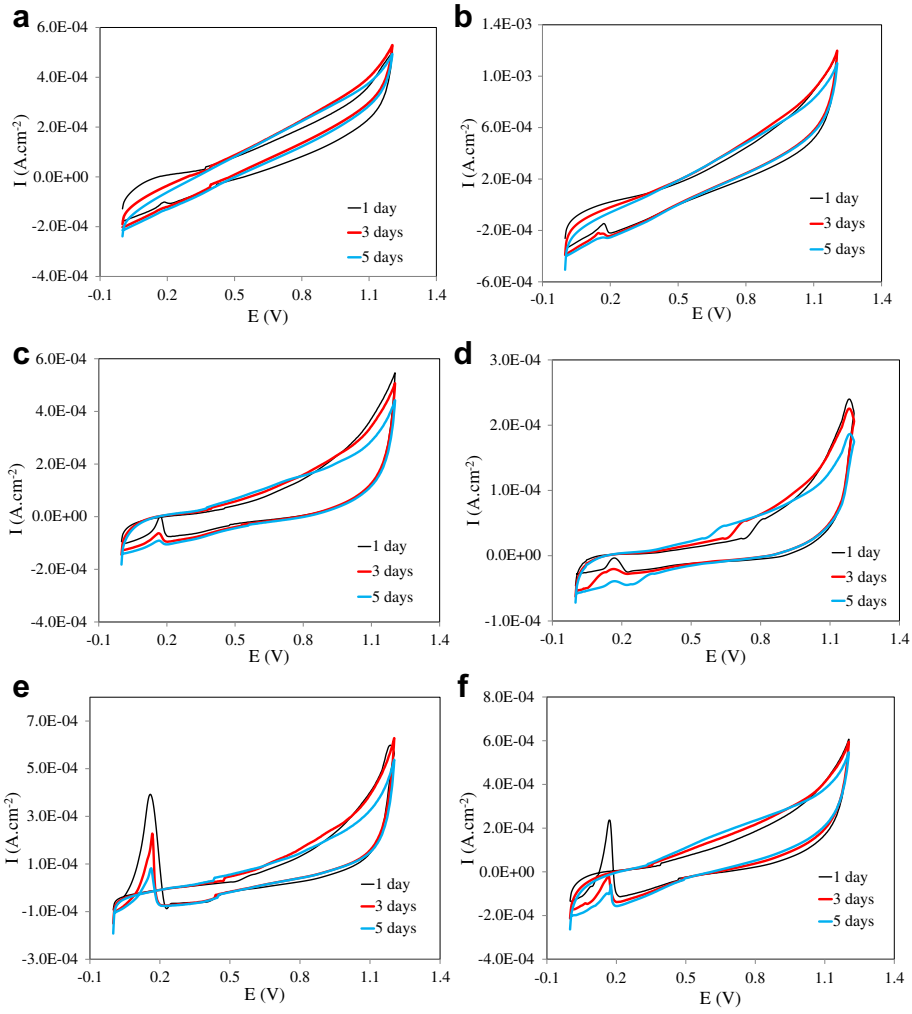

Fig. 2. Cyclic voltammograms of the ABS–graphite–MWNT composites after different immersion times in 0.5 M H_2SO_4 + 2 ppm HF solution at 70 °C: a) S0; b) S1; c) S2; d) S3; e) S4; f) S5.

US Department of Energy (DOE) has defined the benchmark for electrical conductivity of composite bipolar plates as 100 S cm^{-1} without specifying, though, if it is the in-plane or the through-plane value. In order to complement the electrical characterization of the composites, we also performed in-plane electrical conductivity measurements. The results are shown in Fig. 3. Due to the little effect that the immersion in 0.5 M H_2SO_4 + 2 ppm HF solution at 70 °C had on the through-plane conductivity of the composites (Fig. 1), the measurements were made only with specimens that were not immersed in the electrolyte.

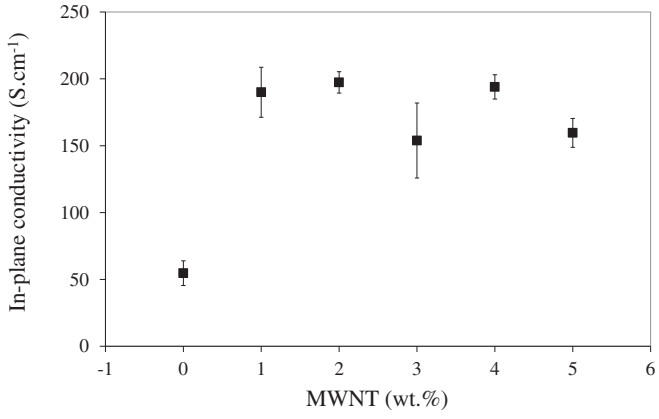

Fig. 3. In-plane electrical conductivity of the composites plotted as a function of the MWNT content.

The results follow the same trend observed for the through-plane measurements but the values are quite higher. MWNT addition led to a significant increase of the conductivity. The values reached 200 S cm^{-1} for some of the S1 and S2 composites. The highest mean value was observed for the S2 composites. As observed for the through-plane measurements, there is a tendency of reducing these values for higher MWNT concentrations which is more accentuated for the S3 composites. Once again, we hypothesize that MWNT clustering can give rise to this behavior. In order to achieve a physical confirmation of this assumption, SEM micrographs of the fractured composites were obtained. The results will be shown later in Figs. 8 and 9. It is noteworthy that the electrical conductivity of the ABS–graphite composites was significantly improved by adding the MWNTs. Furthermore, this performance was achieved without any prior surface treatment of the MWNTs. It is often reported that specific surface treatments can greatly enhance the dispersibility of carbon nanotubes within polymer matrices, favoring the formation of conductive paths, thus improving the electrical conductivity of the composite [47,48]. In

this regard, the results presented here can be further improved by properly treating the surface of the MWNTs. However, this was not the aim of the present work. We aimed to assess the corrosion properties of the ABS–graphite–MWNT composites and verify possible correlations with the through-plane electrical conductivity. This issue is addressed in the next section.

3.2. Electrochemical impedance spectroscopy (EIS)

Nyquist plots of the ABS–graphite–MWNT composites after different periods of immersion in 0.5 M H_2SO_4 + 2 ppm HF solution at 70 °C are shown in Fig. 4. EIS is an attractive technique to study the corrosion processes of electrical conductors in aqueous electrolytes due to the low amplitude of the perturbation signal that allows the monitoring of the evolution of the electrochemical behavior of the electrode with time, without altering its surface properties [49]. The plots in Fig. 4a are referred to the S0 composite. It is seen that the Nyquist plots are characterized by one capacitive loop in the low frequency domain whose radius present a slight decrease with the immersion time. The diameter of the Nyquist plot along the real axis is associated with the charge transfer resistance of the material, thereby indicating its corrosion resistance [50]. In this regard, the S0 composite was found to be relatively stable in the electrolyte up to the end of the test. The impedance values remained high from 1 to 5 days of immersion and the diameter of the capacitive loop was marginally flattened. The same tendency was observed for the S1 composite but the impedance reduction is more accentuated (Fig. 4b). The S2 composites presented the same tendency of the S0 composites but the impedance values are lower for all immersion times (Fig. 4c). It can be assumed that the incorporation of the MWNTs did not increase the instability of the ABS–graphite composite in the electrolyte. This behavior was significantly altered, though, for higher MWNT loadings. As can be seen in Fig. 4d, the S3 composite presented a sharp decrease of the diameter of the capacitive loop of the Nyquist after 5 days of immersion. The shape of the Nyquist plot was also different from that observed for the S0, S1 and S2 composites, especially after 5 days. After 1 and 3 days of immersion the Nyquist is characterized by a capacitive loop whose radius is relatively stable. However, after 5 days there was a sharp decrease of the impedance and typical Warburg impedance appears at low frequencies as denoted by the diffusion tail (slope of 45°), suggesting that diffusion processes are active [51]. The presence of the diffusion tail was not observed for the S4 and S5 specimen as seen in Fig. 4e and f. However, the same trend of reduction of the diameter of the Nyquist plot is markedly present. These results suggest that the S3, S4 and S5 were more prone to corrosion than the S2, S1 and S0 composites.

In order to give a more quantitative interpretation of the impedance response, the experimental data were fitted using equivalent electrical circuits (EECs) through a non-linear least

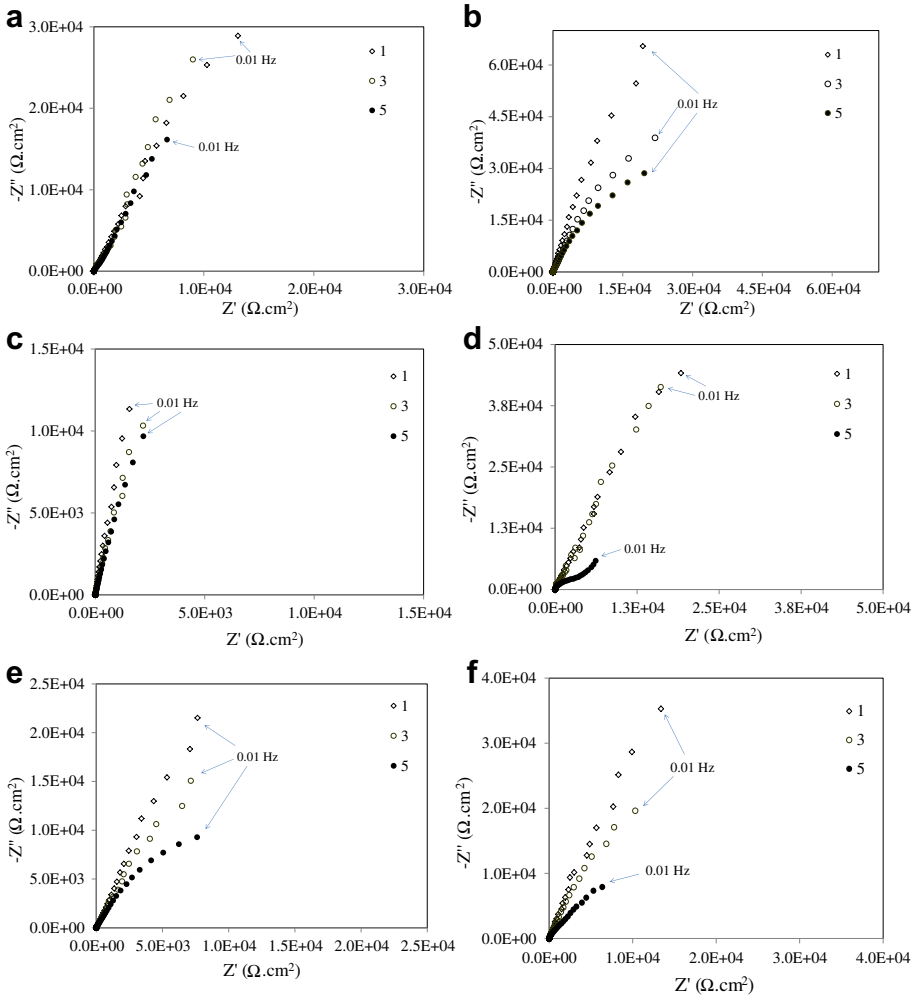

Fig. 4. Nyquist plots of the ABS–graphite–MWNT composites after different immersion times in 0.5 M H_2SO_4 + 2 ppm HF solution at 70 °C: a) S0; b) S1; c) S2; d) S3; e) S4; f) S5.

Table 2
Equivalent circuit parameters for the ABS–graphite–MWNT composites for 1, 3 and 5 days of immersion.

Time (days)	Composite	Parameters							
		R_1 ($\Omega\cdot cm^2$)	Q_1 ($10^{-4}\cdot F\cdot cm^{-2}\cdot s^{\alpha-1}$)	R_2 ($k\Omega\cdot cm^2$)	n_1	Q_2 ($10^{-4}\cdot F\cdot cm^{-2}\cdot s^{\alpha-1}$)	R_3 ($k\Omega\cdot cm^2$)	n_2	W_1 ($10^{-4}\cdot\Omega^{-1}\cdot cm^{-2}\cdot s^{-0.5}$)
1	S0	1.94	1.29	2.43	0.91	1.14	429	0.74	–
	S1	2.97	1.09	11.7	0.93	0.30	638	0.80	
	S2	2.59	9.09	337	0.94	–	–	–	–
	S3	1.79	0.99	5.64	0.93	0.70	506	0.76	–
	S4	2.63	2.53	2.62	0.86	0.91	502	0.75	–
	S5	2.66	1.61	4.64	0.90	0.76	252	0.83	–
3	S0	1.86	1.31	2.90	0.91	1.77	364	0.83	–
	S1	2.91	1.20	5.74	0.91	0.73	192	0.81	
	S2	2.40	9.41	137	0.92	–	–	–	–
	S3	1.92	0.95	5.62	0.93	0.97	372	0.82	–
	S4	2.39	3.72	5.79	0.83	1.43	74.5	0.96	–
	S5	2.50	2.68	2.96	0.87	0.85	113	0.78	–
5	S0	1.77	1.92	1.83	0.88	2.57	167	0.81	–
	S1	2.85	1.57	7.55	0.91	0.77	105	0.80	
	S2	2.31	9.23	7.08	0.92	0.88	130	0.85	–
	S3	1.79	1.10	0.81	0.92	0.31	2.32	0.84	$4.33\cdot10^{-4}$
	S4	2.46	4.15	5.01	0.82	1.87	30.5	0.92	–
	S5	2.44	3.31	3.85	0.85	3.58	35.2	0.76	–

square (NLLS) fitting procedure. The capacitive behavior was simulated using constant phase elements (CPEs) instead of pure capacitors accounting for the inhomogeneity of the material surfaces [52]. The parameters obtained from the modeling of the EIS data are summarized in Table 2. Q and n are the magnitude and the exponent of the constant phase element. The CPE impedance is described by equation (1) [53]. Q is identified with the capacitance of the CPE, $j\omega$ is the complex variable for sinusoidal perturbations, ω is the angular frequency and n gives information about the nature of the nature of the CPE. For a pure capacitor $n = 1$ and $n = 0.5$ for a mass transfer process [54]. The EECs used to fit the experimental data are shown in Fig. 5. Nyquist plots of the ABS–graphite–MWNT composites after 1, 3 and 5 days of immersion are shown in Fig. 6 for both experimental and fitted data. The quality of the fitting procedure is clearly demonstrated.

$$Z_{CPE} = [Q(j\omega)^n]^{-1}$$

The EEC shown in Fig. 5a yielded the best fitting to the experimental data of the S0 and S1 composites for the whole period of immersion. Alias and Brown [55] used the same model to simulate the EIS response of carbon fiber–epoxy and carbon fiber–vinyl ester composites. In this model R_1 is the electrolyte resistance; Q_1 and R_2 are related to the composite/electrolyte interface where R_2 is the pore resistance to the penetration of electrolyte and Q_1 models the associated capacitance. Q_2 and R_3 are due to the charge transfer reactions which occur within the pores due to the penetration of the electrolyte. This model was also successfully used to model the EIS data of polyvinylidene fluoride–graphite composites in a simulated PEM fuel cell environment [15]. As seen in Table 2 there is a tendency of reduction of the values of the R_2 and R_3 after 5 days of immersion. This behavior corresponds to a decrease of the corrosion resistance of the composite due to the penetration of electrolyte with time. The n values are close to 0.9 for all the immersion times which is typical of a capacitive response [56], suggesting that the composite remains relatively stable during the test. The increase of Q_1 and Q_2 from 1 to 5 days can be also explained by the penetration of electrolyte through the pores of the composite, thus exposing higher surface area to the corrosive medium [15].

The EEC shown in Fig. 5a did not provide the best fitting to the experimental data of the S2 composites. The addition of 2 wt.% of MWNTs to the ABS–graphite composites altered the electrochemical behavior. The circuit shown in Fig. 5b provided the best fitting for the EIS response of the S2 composites after 1 and 3 days of immersion. This model presents only one time constant instead of the two time constants modeled by the circuit shown in Fig. 5a. In this model, R_1 is the electrolyte resistance. Q1 and R2 model the charge transfer reactions in the interface between the electrolyte and the conductive surface of the composite. This difference probably arises from the fact that the addition of 2 wt.% of MWNTs would be effective at connecting neighbor graphite particles, diminishing the intrinsic voids in the structure of the S2 composites. For the S1

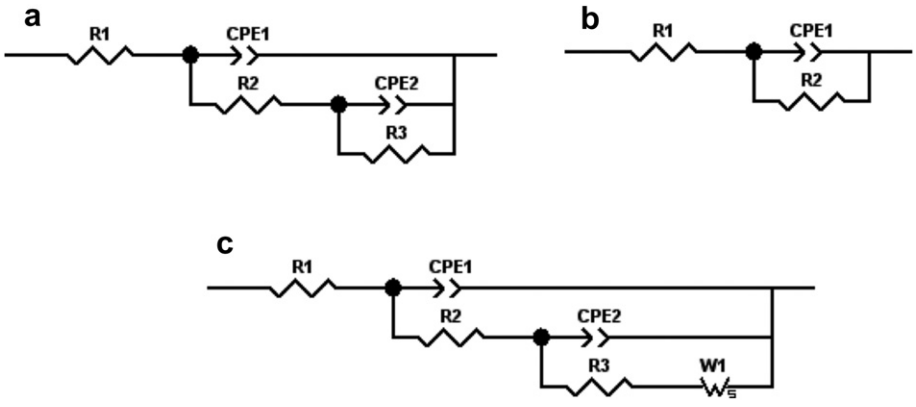

Fig. 5. EECs used to fit the impedance data of the different composites.

composites the amount of carbon nanotubes would not be sufficient to impart the same behavior. As a result, the time constant modeling the resistance and capacitance of the pores was not relevant during the initial timeframe of the test. This would also have a beneficial effect on the electrical conductivity of the composite. In fact, the through-plane electrical conductivity of the S2 composites was significantly higher than that of the S0 composites. However, after 5 days, this model did not provide a good fitting for the experimental data. The electrochemical behavior of the S2 composites evolved and the EEC shown in Fig. 5a gave the best fitting to the EIS data after 5 days of immersion. Then, as already discussed for the S0 and S1 composites, the composite/electrolyte interface was modeled by a pore resistance (R_2) and its associated capacitance (Q_1). This time constant was developed probably due to the penetration of electrolyte for longer immersion times, increasing the area exposed to the electrolyte. It is noteworthy that the charge transfer resistance decreased from 1 to 5 days of immersion. However, it remained relatively high up to the end of the test, confirming the stability of the S2 composites. This behavior was apparent in the Nyquist plots of Fig. 4c.

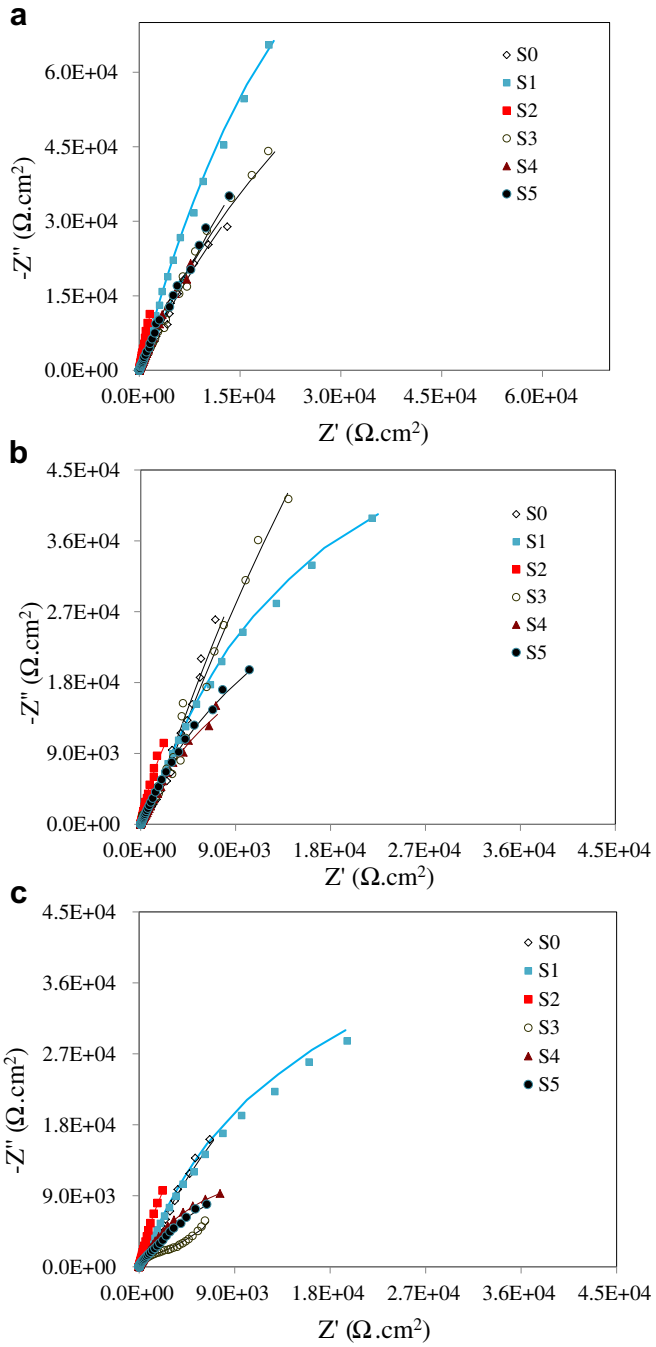

Fig. 6. Nyquist plots of the ABS–graphite–MWNT composites after different periods of immersion in 0.5 M H_2SO_4 + 2 ppm HF solution at 70 °C: a) 1 day; b) 3 days; c) 5 days; solid lines indicate the fitted curves.

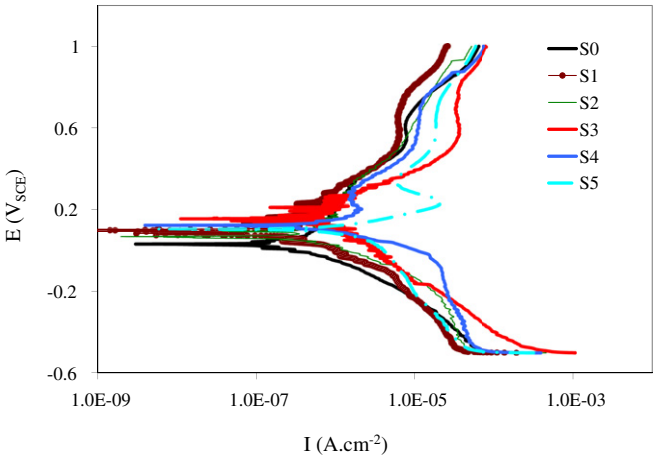

Fig. 7. Potentiodynamic polarization curves of the ABS–graphite–MWNT composites after 5 days of immersion in 0.5 M H_2SO_4 + 2 ppm HF solution at 70 °C.

The EEC shown in Fig. 5a was successfully employed to fit the experimental data of the S3 composites after 1 and 3 days of immersion. In this regard, the same considerations concerning the physical meaning of the fitting parameters discussed for the S0 and S1 composites can be applied here. The most striking feature is the reduction of the charge transfer resistance (R_3) and the increase of the associated capacitance (Q_2) from 1 to 3 days, denoting the deterioration of the corrosion resistance with time. However, R_3 is still high after 3 days, approaching the charge transfer resistance of the S0 composite. Conversely, after 5 days R_3 sharply decreased and a new time constant evolved in the system. The EEC shown in Fig. 5c provided the best fitting for the S3 composites after 5 days of immersion. A Warburg impedance (W) was introduced to model the EIS response in the low frequency domain. W_1 is the Warburg coefficient. The diffusion tail that developed after 5 days (see the Nyquist plots in Fig. 4d), forming a line with slope of approximately 45° to the real axis is characteristic of the semi-infinite length Warburg impedance [57]. This parameter is related to diffusion-controlled processes [58]. This feature was not observed for the EIS response of the S2 composites. It is hypothesized that the increase of MWNT concentration can give rise to clusters that favor the penetration of the electrolyte and the onset of diffusion of aggressive species through the pores of the composite, leading to a sharp decrease of the corrosion resistance. In this context, it is possible to

Table 3
Electrochemical parameters determined from the polarization curves shown in Fig. 7.

Composite	E_{corr} (VSCE)	I_{corr} (μA·cm^{-2})
S0	0.04	0.50
S1	0.10	0.95
S2	0.07	1.25
S3	0.16	1.44
S4	0.13	2.59
S5	0.11	3.33

ensure that the addition of the MWNTs to the ABS–graphite composites improves the through-plane electrical conductivity as shown in Fig. 1. Notwithstanding, it can create, depending on the concentration, pathways to the diffusion of aggressive corrosive species. Hence, the composite is prone to deterioration in the PEM fuel cell environment which can decrease the electrical performance with time. The susceptibility of MWNTs to electrochemical oxidation in PEM fuel cell environments has been recognized by several authors, especially at high potentials [22,23]. The results obtained in this work evidence that the deterioration of the corrosion resistance of MWNT-added ABS–graphite composites can take place even though electrochemical oxidation was not perceived to be relevant for the electrical conductivity of the composites according to the experimental conditions employed here.

The fitting procedure for the S4 and S5 composites was successfully conducted through the use of the EEC shown in Fig. 5a. This EEC provided the best fitting to the experimental data for all the immersion times. In this regard, the EIS response of these composites resembles that of the S0 and S1 ones. Additionally, the same tendency of reduction of the values of R_3 with time was also observed for the S4 and S5 composites, indicating the decrease of corrosion resistance with the elapsed time. It has to be emphasized, though, that the charge transfer resistance was much lower for the S4 and S5 in comparison with the S0 and S1 composites as well as the impedance values, especially for 3 and 5 days of immersion. This is clearly seen in the Nyquist plots shown in Fig. 6. This lack of stability of the S4 and S5 composites can be due to the formation of pathways to the penetration of the electrolyte as a result of the agglomeration of the MWNTs. The relatively high content of MWNTs in the S4 and S5 composites favors this situation. For the S1 and S2 composites the decrease of the charge transfer resistance with time was much less intense than for the S4 and S5 composites.

3.3. Potentiodynamic polarization curves

Potentiodynamic polarization curves of the ABS–graphite–MWNT composites after 5 days of immersion in 0.5 M H_2SO_4 + 2 ppm HF solution at 70 °C are shown in Fig. 7. The corresponding electrochemical parameters are summarized in Table 3. The corrosion current densities (I_{corr}) were obtained considering the cathodic branch of the polarization curves.

The results show that the corrosion potential (E_{corr}) was shifted to nobler values with the addition of MWNTs. However, the corrosion current densities (I_{corr}) were directly proportional to the MWNT concentration, increasing for higher MWNT contents. Thus, it is possible to infer that the corrosion resistance of the composites was impaired by the addition of the MWNTs. This result corroborates the indications of the EIS measurements. A similar behavior

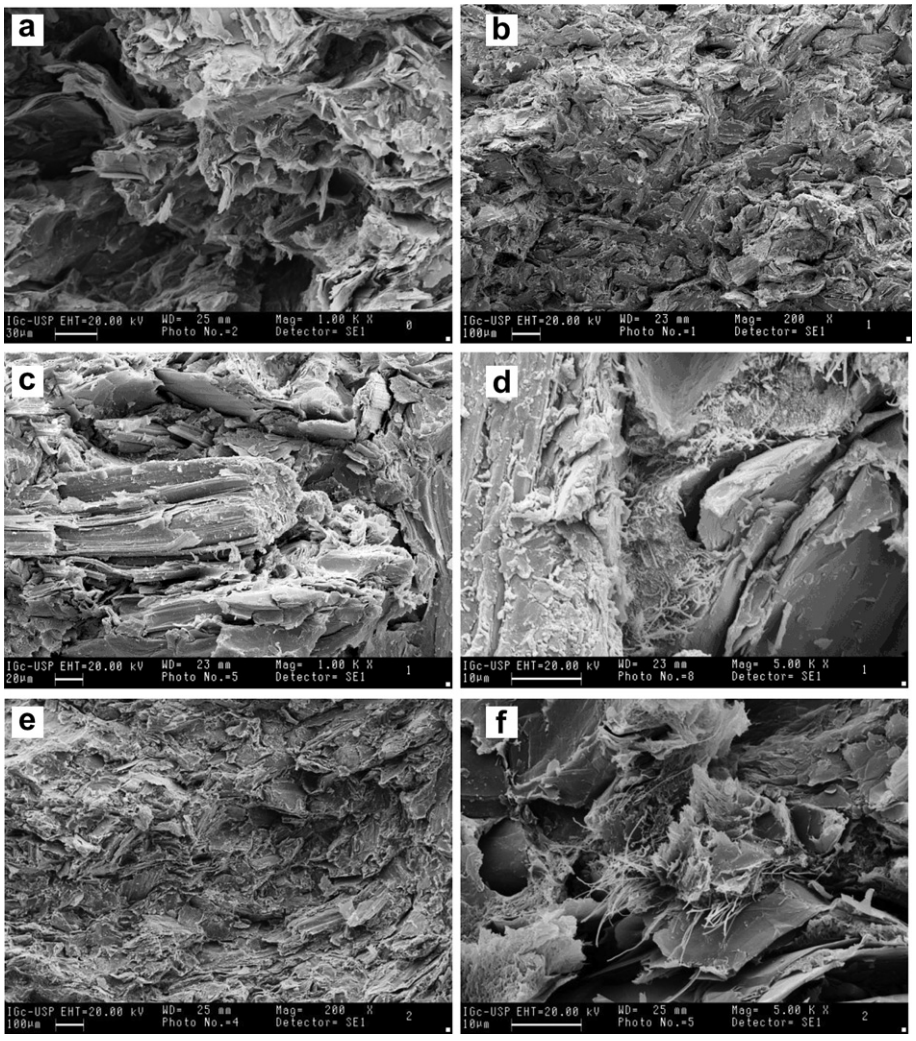

Fig. 8. SEM micrographs of the fracture surfaces of the ABS–graphite–MWNT composites: a) S0; b), c) and d) S1; e) and f) S2.

was also observed by Kakati et al. [9] and Antunes et al. [15] for polymer–graphite–carbon black composite bipolar plates. A possible explanation is the relatively higher electrochemical instability of carbon black in comparison with that of graphite [9]. From the results obtained here, we found that the incorporation of the highly conductive MWNTs has a similar effect on the corrosion behavior of the ABS–graphite composites. Notwithstanding, the I_{corr} values are low, suggesting that the deterioration occurs at a slow rate.

3.4. SEM micrographs

Representative SEM micrographs of the fracture surfaces of the different ABS–graphite–MWNT composites are shown in Figs. 8 and 9. The morphology of the S0 composite is shown in Fig. 8a. The cross section of this composite reveals that some voids are distributed within the structure. The voids make the transport of electrons more difficult, as less conductive paths between neighboring graphite particles are formed. In this regard, the through-plane electrical conductivity would not be favored in this structure. As shown in Fig. 1, the low values of this property for the S0 composites confirm this assumption.

The structures of the S1 and S2 composites were apparently more homogeneous, showing fewer voids between the conductive particles than the S0 composite. The micrographs shown in Fig. 8b and c show the relative compactness of the S1 composite. MWNT clustering was not perceived in the S1 composites. The nanotubes were distributed within the structure as shown in the representative micrograph of Fig. 8d where some MWNTs are found in the central part of the figure. This morphology would favor the corrosion performance of the composite and also the increase of electrical conductivity due to the addition of the highly conductive MWNTs.

The micrograph in Fig. 8e is a global view of the fracture surface of the S2 composite, revealing the apparent compactness of the structure. The image in Fig. 8f is a closer view of the top right region shown in Fig. 7e. The presence of the MWNTs in the S2 composite is evident which would account for its higher through-plane electrical conductivity and lower impedance values in comparison with the S0 composite. However, for long periods in contact with the PEM fuel cell electrolyte, it is likely that the more internally defective structure of the S0 composite would be more prone to corrosion than the more homogeneous morphology of the S2 composite. This would explain the results obtained from the EIS measurements which indicated that the reduction of the charge transfer resistance of the S0 composites was proportionally more accentuated than that of the S2 composites after 5 days of immersion.

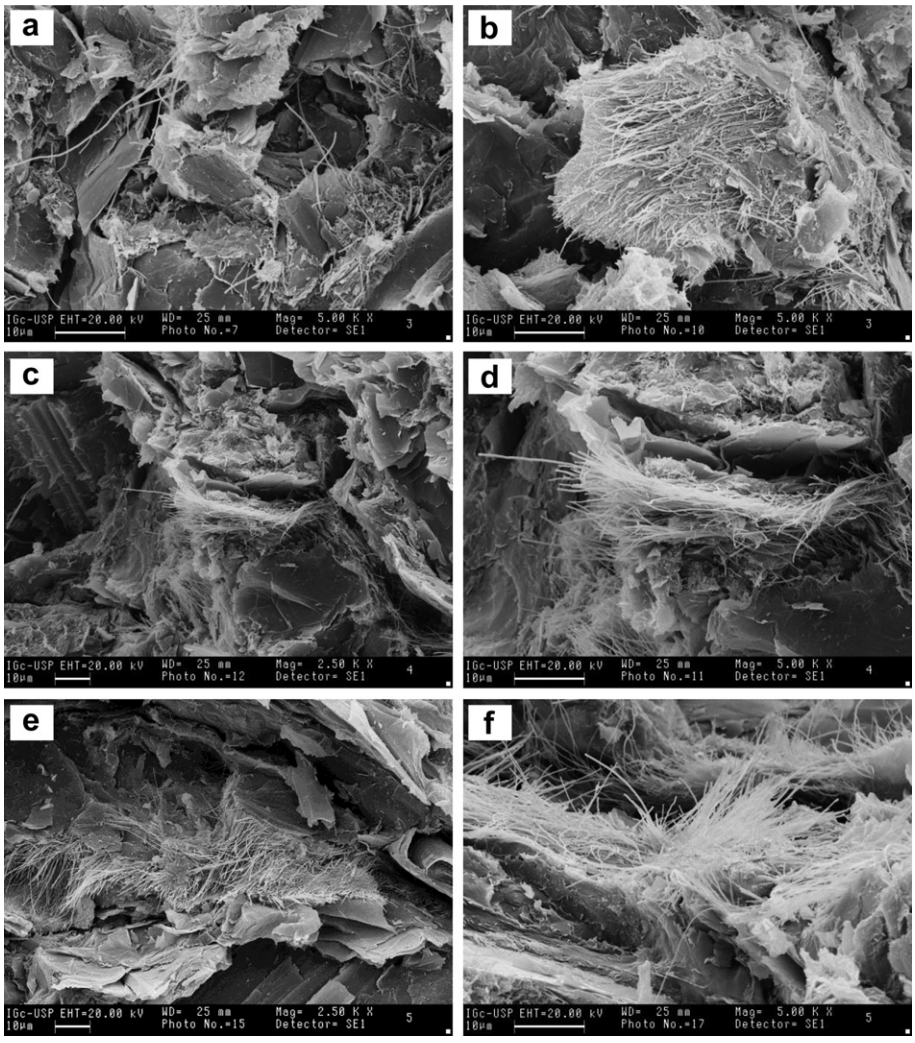

Fig. 9. SEM micrographs of the fracture surfaces of the ABS–graphite–MWNT composites: a) and b) S3; c) and d) S4; e) and f) S5.

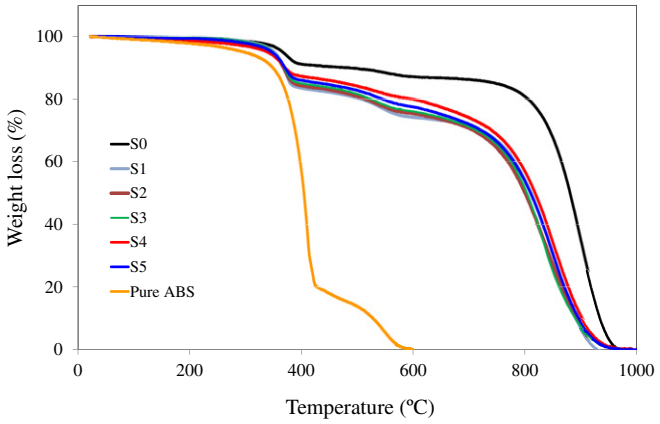

Fig. 10. TGA curves of the ABS–graphite–MWNT composites.

The higher MWNT loading of the S3 composite yielded the formation of more clusters throughout its structure than was observed in the S2 composite. Some examples are shown in Fig. 9a and especially in Fig. 9b. The agglomeration of high surface area MWNTs renders the wetting of the conductive fillers by the binders more difficult. As a result, the penetration of the electrolyte is favored and the composite would be more prone to corrosion. This would explain the high decrease of the charge transfer resistance of the S3 composite with time as indicated by the fitting of the EIS experimental data. The formation of diffusion controlled processes after 5 days of immersion can be also a consequence of the MWNTs clustering.

As the MWNT concentration increased the formation of bundles became more frequent. This is observed for the S4 and S5 composites as shown in Fig. 9c–f. These composites presented a high decrease of the charge transfer resistance with time, as indicated from the fitting procedure of the experimental EIS data. This behavior resembles that of the S3 composite and would be also explained by the formation of pathways to the penetration of the electrolyte through the heterogeneous MWNTs clustering regions. Moreover, the higher concentration of the conductive nanofillers would lead to the increase of the corrosion current densities observed in the potentiodynamic polarization curves of Fig. 7. In the same regard, the electrical conductivity can be adversely affected by the presence of the MWNT clusters. This was especially observed for the S3 composites which were also the most prone to corrosion.

3.5. Thermal stability

TGA curves of the ABS–graphite–MWNT composites are shown in Fig. 10. The residue at 600 °C was almost zero for the pure ABS resin. The S0 composite presented the highest thermal stability. The onset temperature for thermal decomposition was increased in comparison with the pure polymer matrix and the weight loss at 600 °C was only around 13%. The incorporation of MWNTs reduced the thermal stability of the ABS–graphite composite. The onset temperature for thermal decomposition and the weight loss at 600 °C were proportionally higher for the MWNT-containing composites. However, there were only slight differences between the thermal stabilities of the S1, S2, S3, S4 and S5 composites. This behavior indicates that the addition of MWNTs has an adverse effect on the thermal stability of the ABS–graphite composite. Nevertheless, the thermal stability is little affected when the MWNT concentration increases from 1 wt.% to 5 wt.%. Yang et al. [59] observed that single walled carbon nanotubes decreased the thermal stability of ABS. They suggested that carbon nanotubes destabilize the ABS polymer by participating in the radical degradation initiation process of the resin. Despite the obvious decrease of thermal stability imparted by the addition of MWNTs, the weight loss remained very small up to 300 °C. This temperature can be considered safe for practical purposes if one considers the application of these composites in PEMFCs [60].

4. Conclusions

The corrosion resistance and thermal stability of ABS–graphite composites with different was evaluated as a function of MWNT concentration. Through-plane and in-plane electrical conductivities of the composites were also determined. Electrochemical oxidation of the MWNT was not significant to electrical conductivity of the composites as shown by the cyclic voltammograms and through-plane measurements of the composites after immersion in the electrolyte. EIS measurements showed that the corrosion resistance was dependent on the MWNT concentration. The incorporation of 2 wt.% of MWNTs provided the best compromise between through-plane electrical conductivity and corrosion resistance. For higher MWNT loadings the corrosion resistance decreased and there was no significant gain in the electrical conductivity. SEM micrographs of the cross sections of the fractured surfaces of the composites revealed that the formation of MWNT clusters can be responsible for depressing the corrosion resistance and also the electrical conductivity. Potentiodynamic polarization curves confirmed the EIS results, showing that the corrosion current densities of the composites increased with the MWNT concentration. The thermal stability of the composites was also depressed with the addition of the MWNTs as evidenced by the TGA curves. Nevertheless, the weight loss at 300 °C was negligible for all the MWNT-added composites which can be considered a suitable performance for application in PEM fuel cells.

Acknowledgments

The authors are grateful to CNPq (The Brazilian Research Council) for the financial support to this work (Project 558134/2008-4). Mara C. L. de Oliveira is thankful for the post-doctoral grant (Proc. 150396/2009-0).

References

[1] R.A. Antunes, M.C.L. De Oliveira, G. Ett, V. Ett, J. Power Sources 196 (2011) 2945–2961.
[2] M.C.L. De Oliveira, G. Ett, R.A. Antunes, J. Power Sources 206 (2012) 3–13.
[3] R.A. Antunes, M.C.L. Oliveira, G. Ett, V. Ett, Int. J. Hydrogen Energy 35 (2010) 3632–3647.
[4] H. Wang, J.A. Turner, Fuel Cells 10 (2010) 510–519.
[5] E. Dur, O.N. Cora, M. Koç, Int. J. Hydrogen Energy 36 (2011) 7162–7173.
[6] W. Jin, K. Feng, Z. Li, X. Cai, L. Yu, D. Zhou, J. Power Sources 196 (2011) 10032–10037.
[7] F.A. De Brujin, V.A.T. Dam, G.J.M. Janssen, Fuel Cells 8 (2008) 3–22.
[8] S.R. Dhakate, R.B. Mathur, S. Sharma, M. Borah, T.L. Dhami, Energy Fuels 23 (2009) 934–941.
[9] B.K. Kakati, D. Sathiyamoorthy, A. Verma, Int. J. Hydrogen Energy 35 (2010) 4185–4194.
[10] J. Wang, G. Yin, Y. Shao, S. Zhang, Z. Wang, Y. Gao, J. Power Sources 171 (2007) 331–339.
[11] M.-X. Wang, Q. Liu, H.-F. Sun, N. Ogbeifun, F. Xu, E.A. Stach, J. Xie, Mater. Chem. Phys. 123 (2010) 761–766.
[12] H.-S. Oh, K.H. Lim, B. Roh, I. Hwang, H. Kim, Electrochim. Acta 54 (2009) 6515–6521.
[13] H.-T. Fang, C.-G. Liu, F. Li, M. Liu, H.-M. Cheng, Chem. Mater. 16 (2004) 5744–5750.
[14] Y. Yang, Z.G. Lin, J. Appl. Electrochem. 25 (1995) 259–266.
[15] R.A. Antunes, M.C.L. De Oliveira, G. Ett, Int. J. Hydrogen Energy 36 (2011) 12474–12485.
[16] S.-H. Liao, M.-C. Hsiao, C.-Y. Yen, C.-C.M. Ma, S.-J. Lee, A. Su, M.-C. Tsai, M.-Y. Yen, P.-L. Liu, J. Power Sources 195 (2010) 7808–7817.
[17] S.C. Tjong, Energy Environ. Sci. 4 (2011) 605–626.

[18] Q. Yin, K.-N. Sun, A.-J. Li, L. Shao, S.-M. Liu, C. Sun, J. Power Sources 175 (2008) 861–865.
[19] L. Li, Y. Xing, J. Power Sources 178 (2008) 75–79.
[20] X. Wang, W. Li, Z. Chen, M. Waje, Y. Yan, J. Power Sources 158 (2006) 154–159.
[21] L. Li, Y. Xing, J. Electrochem. Soc. 153 (2006) A1823–A1828.
[22] Y. Shao, G. Yin, J. Zhang, Y. Gao, Electrochim. Acta 51 (2006) 5853–5857.
[23] C.-C. Hung, P.-Y. Lim, J.-R. Chen, H.C. Shih, J. Power Sources 196 (2011) 140–146.
[24] C.-T. Hsieh, W.-M. Hung, W.-Y. Chen, Int. J. Hydrogen Energy 35 (2010) 8425–8432.
[25] H. Lv, N. Cheng, S. Mu, M. Pan, Electrochim. Acta 58 (2011) 736–742.
[26] R.F. Silva, D. Franchi, A. Leone, L. Pilloni, A. Masci, A. Pozio, Electrochim. Acta 51 (2006) 3592–3598.
[27] R. Tian, J. Sun, L. Wang, Int. J. Hydrogen Energy 31 (2006) 1874–1878.
[28] T. Fukutsuka, T. Yamaguchi, S.-I. Miyano, Y. Matsuo, Y. Sugie, Z. Ogumi, J. Power Sources 174 (2007) 199–205.
[29] H. Xu, Y. Song, H.R. Kunz, J.M. Fenton, J. Power Sources 159 (2006) 979–986.
[30] Y. Shao, G. Yin, Z. Wang, Y. Gao, J. Power Sources 167 (2007) 235–242.
[31] B.D. Cunningham, J. Huang, D.G. Baird, J. Power Sources 165 (2007) 764–773.
[32] B.K. Kakati, V.K. Yamsani, K.S. Khathathreyan, D. Sathiyamoorthy, A. Verma, Carbon 47 (2009) 2413–2418.
[33] P.H. Maheshwari, R.B. Mathur, T.L. Dhami, J. Power Sources 173 (2007) 394–403.
[34] Fuel Cell Technologies Program Multi-Year Research, Development and Demonstration Plan, U.S. Department of Energy, Fuel Cell Technologies Program, Washington, DC, 2007.
[35] L.-G. Xia, A.-J. Li, W.-Q. Wang, Q. Yin, H. Lin, Y.-B. Zhao, J. Power Sources 178 (2008) 363–367.
[36] X. Jiang, L.T. Drzal, J. Power Sources 218 (2012) 297–306.
[37] M. Yousefi, F. Gholamian, D. Ghanbari, M. Salavati-Niasari, Polyhedron 30 (2011) 1055–1060.
[38] H. Ma, L. Tong, Z. Xu, Z. Fang, Y. Jin, F. Lu, Polym. Degrad. Stab. 92 (2007) 720–726.
[39] C.M. Hong, S.H. Park, Y.J. Lee, United States Patent Application 20080268322.
[40] L. Du, S.C. Jana, J. Power Sources 172 (2007) 734–741.
[41] T. Derieth, G. Bandlamudi, P. Beckhaus, C. Kreuz, F. Mahlendorf, A. Heinzel, J. New Mater. Electrochem. Syst. 11 (2008) 21–29.
[42] S.R. Dhakate, S. Sharma, N. Chauhan, R.K. Seth, R.B. Mathur, Int. J. Hydrogen Energy 35 (2010) 4195–4200.
[43] J.H. Lee, Y.K. Jang, C.E. Hong, N.H. Kim, P. Li, H.K. Lee, J. Power Sources 193 (2009) 523–529.
[44] Y. Pan, L. Li, S.H. Chan, J. Zhao, Composites: Part A 41 (2010) 419–426.
[45] R.H. Baughman, A.A. Zakhidov, W.A. de Heer, Science 297 (2002) 787–792.
[46] N. Grossiord, J. Loos, O. Regev, C.E. Koning, Chem. Mater. 18 (2006) 1089–1099.
[47] S.-H. Liao, C.-H. Hung, C.-C.M. Ma, C.-Y. Yen, Y.-F. Lin, C.-C. Weng, J. Power Sources 176 (2008) 175–182.
[48] S.-H. Liao, C.-Y. Yen, C.-C. Weng, Y.-F. Lin, C.-C.M. Ma, C.-H. Yang, M.-C. Tsai, M.-Y. Yen, M.-C. Hsiao, S.-J. Lee, X.-F. Xie, Y.-H. Hsiao, J. Power Sources 185 (2008) 1225–1232.
[49] K. Jüttner, Electrochim. Acta 35 (1990) 1501–1508.
[50] M.C. Turhan, R. Lynch, M.S. Killian, S. Virtanen, Electrochim. Acta 55 (2009) 250–257.
[51] V. Barranco, S. Feliu Jr., S. Feliu, Corr. Sci. 46 (2004) 2221–2240.
[52] C. Liu, Q. Bi, A. Leyland, A. Matthews, Corr. Sci. 45 (2003) 1243–1256.
[53] B.A. Boukamp, Solid State Ionics 18-19 (1986) 136–140.
[54] A.C. Bastos, M.G. Ferreira, A.M. Simões, Corr. Sci. 48 (2006) 1500–1512.
[55] M.N. Alias, R. Brown, Corr. Sci. 35 (1993) 395–402.
[56] L.E.M. Palomino, P.H. Suegama, I.V. Aoki, Z. Pászti, H.G. de Melo, Electrochim. Acta 52 (2007) 7496–7505.
[57] J.-M. Hu, J.-T. Zhang, J.-Q. Zhang, C.-N. Cao, Corr. Sci. 47 (2005) 2607–2618.
[58] D. Yang, C. Liu, X. Liu, M. Qi, G. Lin, Curr. Appl. Phys. 5 (2005) 417–421.
[59] S. Yang, J.R. Castilleja, E.V. Barrera, K. Lozano, Polym. Degrad. Stab. 83 (2004) 383–388.
[60] J.W. Kim, N.H. Kim, T. Kuilla, T.J. Kim, K.Y. Rhee, J.H. Lee, J. Power Sources 195 (2010) 5474–5480.